Dynamic Weakening of Sandstone Subjected to Repetitive Impact Loading

L.H. Tong[1,2], **Yang Yu**[1,2], **S.K. Lai**[3,4,*], **C.W. Lim**[5,6]

[1] *Institute of Geotechnical Engineering, School of Civil Engineering and Architecture, East China Jiaotong University, Nanchang, 330013, Jiangxi, P.R. China*

[2] *Jiangxi Key Laboratory of Infrastructure Safety and Control in Geotechnical Engineering, East China Jiaotong University, Nanchang, 330013, Jiangxi, P.R. China*

[3] *Department of Civil and Environmental Engineering, The Hong Kong Polytechnic University, Hung Hom, Kowloon, Hong Kong, P.R. China*

[4] *The Hong Kong Polytechnic University Shenzhen Research Institute, Shenzhen, P.R. China*

[5] *Department of Architecture and Civil Engineering, City University of Hong Kong, Kowloon, Hong Kong, P.R. China*

[6] *City University of Hong Kong Shenzhen Research Institute, Shenzhen, P.R. China*

Abstract

Dynamic weakening is commonly observed when stone is subjected to a single or repetitive impact loading. In a series of impact loading experiments conducted using the split Hopkinson pressure bar system with external confinement pressure, we observe evident nonlinear dynamic response for each impact loading, an accompanying dynamic weakening effect, and significant plastic deformation of the specimen. The dynamic response can be predicted accurately by the nonlinear granular model [*Johnson and Jia, Nature, 437 (2005) 871-874*]. In the framework of statistics, an analytical model for

[*]Corresponding author. E-mail: sk.lai@polyu.edu.hk (S.K. Lai)

dynamic weakening is proposed and it suggests that the weakening effect is induced by the increasing number of broken inter-particle bonds after impact. This is related to a decrease in the dynamic modulus that can be described by introducing a confinement pressure-dependent energy portion parameter μ. A further nonlinear analysis of the experimental data provides detailed insights into the nonlinear dynamic response. The proposed weakening mechanism is based on inter-particle statistics and it comprises a wealth of dynamic regimes, including modulus softening and damage evolution, which can be extended to other granular materials but not limited to rocks.

Keywords: Dynamic weakening, Impact loads, Sandstone, Nonlinear response

1 Introduction

Rock failure induced by dynamic loads has been the subject of extensive experimental and theoretical studies (Li et al., 2017; Xia and Yao, 2015), but the failure mechanism remains unclear. An in-depth understanding of the failure mechanism of rocks subjected to dynamic loads is of great significance to rock engineering that involves safety design and disaster prevention (Brown, 2012; Li et al., 2018). Observation of the evolution of rock damage can provide valuable information on the evaluation and assessment of rock failure (Xu and Dai, 2018; Xu et al., 2016). However, in most circumstances, in-situ dynamic experiments are time consuming, uneconomical, and often impractical.

Unlike static load testing methods, dynamic testing methods are very rarely available and limited. In this regard, the Split Hopkinson pressure bar (SHPB) system is a reliable high-strain rate loading technique suggested by the International Society for Rock Mechanics (Xia and Yao, 2015; Zhou et al., 2012). Li et al. (2018) conducted a series of dynamic tests to study the dynamic characteristics of green sandstone subjected to repetitive impact loading. The frequency spectrum analysis showed that energy can gradually transfer from a high- to a low-frequency component after each impact. It also indicated that there is a significant and cumulative damage in the rock body. Micro-structural observations revealed that micro-cracks are randomly distributed after impact, this also indicated that a different failure mechanism is formed due to a static load (Li et al., 2018). To quantify the impact fatigue behavior of rocks, Wu et al. (2014) adopted a specially designed steel sleeve attached on the SHPB system to investigate the fatigue failure evolution of rocks by applying repetitive impact loading. In addition, a multi-particle crushing apparatus was designed for studying the rock-particle-group under

repetitive impact loading (Huang et al., 2017). On the basis of this study, a better understanding of the rock fragmentation mechanism during the crushing process was achieved. However, rocks are typically found underground, the failure of rocks can be induced by blasting (Kaiser and Cai, 2012; Li et al., 2011) and earthquakes (Du et al., 2018), subjected to a coupled dynamic-static stress state. The deformation and mechanical properties of rocks subjected to coupled loads greatly differ from those caused solely by either static or dynamic loading (Li et al., 2008; Zhu et al., 2012), and thus the process cannot be simply described by either static or dynamic theories alone (Li et al., 2017).

To investigate the mechanical characteristics of rocks buried underground subjected to an impact load, the rocks should be subjected to both dynamic and static loads (Li et al., 2017). The dynamic-static coupled load testing technique was improved by Li et al. (2008) and later by Frew et al. (2010), who further modified the SHPB system to characterize the dynamic properties of hydrostatic pressurized rocks. Kuru grey granite was selected by Hokka et al. (2016) for a systematic study of the mechanical properties and behavior of rocks at a confining pressure up to 225 MPa and at strain rates of 10^{-6} s^{-1} and 600 s^{-1}. They found that the dynamic strength increases with increasing confining pressure and that the strain rate sensitivity decreases under a higher confinement. The tensile failure of rocks was investigated by Wu et al. (2016) by loading the Brazilian disc sample hydrostatically with a modified SHPB system. The tests showed that an increasing confining pressure and loading rate can enhance the dynamic tensile strength. The dynamic fracture behavior of rocks subject to a static pre-load was studied by Chen et al. (2016) using a notched semi-circular bend method. The results demonstrated that an increasing loading rate can weaken the dynamic rock fracture toughness. To experimentally investigate the crack development

for rocks underground under a high confinement induced by excavation, Weng et al. (2018) used a high-speed camera system to capture the cracking and failure processes. It was found that the specimens were fractured due to tensile cracks along the compressional direction at a low confinement, whereas shear cracks can induce fracture at a high confinement. Furthermore, Chen et al. (2018) performed the stress equilibrium assessment in axially constrained tri-axial SHPB tests by using both stress wave analysis and numerical simulations.

Although these investigations can provide preliminary insights into rock failure, the identification of an in-depth mechanism responsible for complex macroscopic behavior is more valuable for quantitative analysis and engineering applications. Dynamic weakening of granular materials under small-amplitude dynamic loads has been observed in several laboratory studies (Espindola et al., 2012; Johnson and Jia, 2005), and inner structural changes were also investigated by a non-invasive probe (sound diffusion) method (Jia, 2004). The weakening mechanism first proposed by Melosh (1979; 1996) can be referred to "*acoustic fluidization*" and it can predict the weakening of faults under dynamic loads. The connection between the small-magnitude failure events and the triggering of earthquakes also verifies the dynamic weakening effect (Johnson et al., 2008). The observation of dynamic weakening on crushed rock particles by applying high strain rate dynamic loads using the SHPB system has been reported (Xia et al., 2013), thereby confirming the reduction of frictional strength and elastic modulus via acoustic fluidization. Granular materials (glass bead assembly) used for laboratory observations are non-cemented and thus differ somewhat from cemented granular rocks, but we believe that the weakening or failure mechanism is similar.

In this study, we examine the dynamic weakening effect of impact loading on sandstone using the SHPB system. We consider the sandstone to have a good grain shape and grain cement. The device used in the present experiment allows us to independently control both confining pressure values and impact loads. It is possible to investigate the influence of confining pressure on the weakening effect of sandstone. The nonlinear effect induced by the applied high-amplitude load is obvious, and the nonlinear stress-strain behavior can be described quantitatively using the nonlinear elastic theory (Brunet et al., 2008; Johnson and Jia, 2005). In addition, we also propose a simple model to account quantitatively for the findings of dynamic weakening phenomena induced by repetitive impact loading.

2 Experimental Setup: Dynamic Weakening of Rocks

We believe that the dynamic weakening of granular-type rocks has a quantitative relation to the energy absorbed by the impacted rocks. To verify this, we conducted a series of impact tests (SHPB) on sandstone (a typical granular-type rock) in a laboratory to understand the relationship between absorbed energy and dynamic weakening. A schematic diagram of the experimental setup is shown in Fig. 1(a). The sandstone specimens were cored from a block (diameter: 48.4 mm; height: 70.5 ± 0.2 mm; Fig. 1(b)) in a quarry in Liuyang, Hunan province, China. The grain size of the specimens varied from 0.2 to 0.5 mm. The density was determined as 2.3 g/cm^3. The elasticity modulus and uniaxial compressive strength were measured with a static deformation test as 8.8 GPa and 71 MPa, respectively. The specimens were first fixed between the incident bar and the transmission bar by applying a pre-stress (2 MPa) provided by the axial compressional

system, and then a confining pressure (2 – 8 MPa) was applied. The striker was driven by the releasing gas from a tank to generate incident stress waves along the incident bar. The magnitude of the incident waves can be controlled by the gas pressure of the tank. To investigate the dynamic weakening of rocks, the specimens should not be fractured under a single impact, and thus the pressure of releasing gas should be reasonably adjusted. The present experiment used a releasing gas pressure of 0.7 and 0.9 MPa. A typical record of the incident, reflected, and transmitted wave forms is given in Fig. 1(c) under the conditions of 0.7 MPa releasing gas pressure and 2 MPa confining pressure. The underground rocks may be subjected to several different types of impact waves. We limit the present study to a compressional impact load in order to characterize the dynamic weakening of rocks. However, the conclusions can be generalized to other circumstances such as shear impact loads.

3 Results and Discussion

We first present the experimental results of stress and strain recorded under two different releasing gas pressure (0.7 and 0.9 MPa) in Fig. 2. The first and second rows in Fig. 2 correspond to a releasing gas pressure of 0.7 MPa (corresponding incident energy, 1.96 J/cm^3) and 0.9 MPa (corresponding incident energy, 2.62 J/cm^3), respectively, and the confining pressure values are 2, 4 and 8 MPa in sequence in each row. The initial dynamic moduli M_0 for the confining pressure 2 MPa, 4 MPa and 8 MPa are 30 GPa, 31 GPa and 33 GPa, respectively. Several repetitive impacts are applied in each case. The unloading curves are not presented herein. As reported in the previous research (Johnson and Jia, 2005), nonlinear behavior is prevalent in granular materials, and a simple

phenomenological nonlinear model can capture the nature of the material nonlinearity. The dynamical stress σ_d can be described as (Johnson and Jia, 2005)

$$\sigma_d = M\varepsilon_d\left(1+\beta\varepsilon_d+\delta{\varepsilon_d}^2+\cdots\right) \tag{1}$$

where ε_d is the dynamic strain, M is the dynamic modulus, β and δ are the first- and second-order dynamic nonlinear parameters for the quadratic and cubic dynamic strains, respectively. The peak value of the dynamic stress shows an obvious decrease after each impact even for the same releasing gas in each impact in a specific case (e.g., 2 MPa confined pressure under 0.7 MPa releasing gas pressure), and this observation indicates a weakening effect. It is obvious to imagine that the modulus M has been softened by the dynamic impact. To successfully apply Eq. (1) to describe the dynamical strain, it is crucial to explore the relationship between modulus and impact load.

From the stress-strain behavior combined with observations on microstructural changes induced by impact loads (Li et al., 2018), the effect of modulus softening can be attributed to the development of micro-cracks. The first step in establishing such a relationship is to determine how the impact affects the appearance and development of micro-cracks. Rock grains are cemented to each other by bonds (Dai et al., 2016; Du et al., 2017; Potyondy and Cundall, 2004) that can sustain friction and compression and also can be broken under a high-amplitude impact load. The number of bonds is obviously huge in terms of a unit volume of the specimen, and an exact treatment for the failure process for each bond during one impact is fairly difficult. Suppose that the broken energy for each bond can be described as a Maxwell statistical distribution model, we have

$$n\left(x\right) = N_0\sqrt{\frac{2}{\pi}}\frac{x^2}{{e_\sigma}^3}\mathrm{e}^{-\frac{x^2}{2{e_\sigma}^2}} \quad \left(x\geq 0\right) \tag{2}$$

where N_0 is the total number of bonds in a unit volume, x is the broken energy, e_σ is the variance of broken energy and $n(x)$ is the number of bonds with the broken energy x. In the previous studies (Espindola et al., 2012; Melosh, 1996), the normal random distribution was selected to explore the distribution of pressure fluctuation, however is discarded here, mainly because we consider the energy to be non-negative in this work. The Maxwell distribution is possibly beneficial, we found that it agrees well with our experimental results according to the following analysis. At the macro-scale, the total broken energy per unit volume of rock can be approximately evaluated as $E_f \propto \sigma_f^{\,2}/(2M_0)$ under the Mohr-Coulomb failure criterion assumption, in which M_0 is the modulus for intact rock, $\sigma_f = k_p\sigma_r + 2k_p c$ where c is the cohesion of rock (5 MPa for the specimen used in our experiment), σ_r is the applied confining pressure and $k_p = \tan^2(45^\circ + \varphi/2)$ with φ as the internal frictional angle (37.8° for the specimen used in the experiment). In most circumstances, the rock undergoes non-brittle failure, but ductile failure may occur, particularly in the condition of a high confining pressure. Therefore, the total broken energy is only a fraction $\mu_1^{\,2}$ of $\sigma_f^{\,2}/(2M)$, resulting in the equation $E_f = \mu_1^{\,2}\sigma_f^{\,2}/(2M)$. From Eq. (2), the average bond broken energy is found to be $\sqrt{8/\pi}e_\sigma$. Consider that only a portion of bonds are broken when the rock fails, the relationship between e_σ and E_f is $e_\sigma = \mu_2^{\,2}\sqrt{\pi/8}\,(E_f/N_0)$ under the condition of $\mu_2 > 1$, hence $e_\sigma = \sqrt{\pi/8}\,\mu^2\sigma_f^{\,2}/(2MN_0)$ with $\mu^2 = (\mu_1\mu_2)^2$. Although μ_1 and μ_2 are two independent parameters, for simplicity we have integrated them into one, μ, which we call the energy portion parameter. Typically, the wavelength is much larger than the bond size, then it is assumed that the

impact energy is uniformly distributed on each bond, as is the energy absorbed by each bond. Therefore, for each impact, the energy absorbed of each bond is E_a/N_0, with E_a being the total absorbed energy per unit volume of rock. We can thus reasonably establish the criterion for bond failure, i.e., $x \le E_a/N_0$. This further leads to the fraction of the bonds to be broken under one impact as

$$\rho\left(E_a,\sigma_r\right)=P\left(x\le\frac{E_a}{N_0}\right)=\int_0^{\frac{E_a}{N_0}}\frac{n(x)}{N_0}dx=\operatorname{erf}\left(\frac{E_a}{\sqrt{2}N_0e_\sigma}\right)-\sqrt{\frac{2}{\pi}}\frac{E_a}{N_0e_\sigma}\mathrm{e}^{-\left(\frac{E_a}{\sqrt{2}N_0e_\sigma}\right)^2} \quad (3)$$

Obviously, the bond number N_0 has no influence on $\rho\left(E_a,\sigma_r\right)$. The only restraint on N_0 is that it is sufficiently large to satisfy the statistical level. An intuitive consideration of relating the broken bond fraction $\rho\left(E_a,\sigma_r\right)$ to the dynamic modulus M is to define $M=M_0\left[1-\rho\left(E_a,\sigma_r\right)\right]$ because the strength of the bond contributes directly to the macroscale dynamic modulus. It is similar to the investigation of acoustic fluidization mechanism of granular materials (Espindola et al., 2012; Melosh, 1996). This is reasonable for small-amplitude impact loads (i.e., for small $\rho\left(E_a,\sigma_r\right)$). However, it cannot stand with $\rho\left(E_a,\sigma_r\right)$ increasing, because the dynamic modulus cannot decrease to zero even for $\rho\left(E_a,\sigma_r\right)$=1. Another model is introduced to describe the modulus softening as $M_i=M_0\exp\left[-\sum_i\rho_i\left(E_{ai},\sigma_r\right)\right]$, where *i* indicates the *i*-th impact. For a small value of ρ_i, this model can be approximately degraded to $M_i=M_0\prod_i\left[1-\rho_i\left(E_{ai},\sigma_r\right)\right]$, which is identical to the equation presented earlier.

Referring back to Eq. (1), the nonlinear quadratic and cubic strain parameters β and

δ are currently unknown. These two parameters should be almost the same for all intact specimens because they depend only on the material type and internal structure of the rock. Through our fittings, $\beta = -55$ and $\delta = -490$ for all intact specimens agree well with the experimental data. Further analysis shows that β is significantly affected by the number of impacts because of the structural change after each impact, whereas δ is nearly independent of the impact number. In addition, both β and δ are independent of confining pressure and impact load amplitude based on the present experimental observations. This is mainly because these nonlinear parameters are primarily determined by their internal structures rather than by their external conditions. Interestingly, for the conditions presented in Fig. 2, β always satisfies the relationship $\beta = -55+5N$ with N as the impact number, see Fig 3(c). The parameter μ introduced is thus the only adjustable parameter to fit the experimental data, because the energy E_a absorbed can be directly obtained from the experiment for each impact in Figs. 3(a) and 3(b). In Fig. 3(a), the energy absorbed is concentrated mainly around 0.62 J/cm^3 for 0.7 MPa releasing gas pressure (corresponding incident energy, 1.96 J/cm^3), which is almost independent of the confining pressure and impact number. However, the average energy absorbed linearly decreases with increasing confining pressure from 2 to 8 MPa under 0.9 MPa releasing gas pressure (corresponding incident energy, 2.62 J/cm^3), as shown in the inset of Fig. 3(b). It implies that the structural damage is gradually suppressed by increasing the confining pressure. In addition, we found that the energy absorbed (the average energy absorbed is shown by the number on each line in Figs. 3(a) and 3(b)) has almost no fluctuations with increasing impact number for all confining pressure we explored.

To capture the dynamic stress-strain behavior under the conditions shown in Fig. 2,

the adjustable parameter μ introduced is fitted in Fig. 3(d). We found that this parameter remains constant at a specific confining pressure impacted by the same dynamic load, which is independent of the impact number. The variation of the confining pressure is also fitted for the releasing gas pressure at 0.7 and 0.9 MPa, and a perfect linear relationship is obtained. Using these parameters thus determined, the dynamic response under repetitive impact loads can be readily explored. Good agreement for all conditions explored is illustrated in Fig. 2 to verify the accuracy of the proposed model in this work.

To quantify the weakening effect due to the impact induced by differences in the releasing gas pressure, we define the decrease in a normalized velocity change as $\Delta C/C_0 = \sqrt{M/M_0} - 1$. The theoretical prediction is presented in Fig. 4. The absolute value of $\Delta C/C_0$ increases in an approximately linear manner with respect to the impact number, and the tendency is significantly affected by the confining pressure, which can also be observed indirectly from Fig. 2. In Fig. 4, the data for the confining pressure 6 MPa is not presented, because this group of data is close to those results obtained under the confining pressure 8 MPa. In general, a higher confining pressure is more likely to suppress the weakening of specimens at the same impact load for all conditions we explored. The dashed black line in Fig. 4(b) indicates a virtual decrease due to the damage of specimens after the second impact. It should be noted that the parameter μ was re-adjusted to 5.6 instead of 4.8 as used in Fig. 2(c), in order to improve the performance of experimental data for the confining pressure 8 MPa under the releasing gas pressure impact load of 0.7 MPa as shown by the solid blue line in Fig. 4(a). This re-adjustment appears to be unreasonable, but it is practically insignificant at the present stage. All other theoretical results, which are obtained based on the parameters achieved from the preceding discussion, agree well with

the experimental observations. Although the research focus of this work is rocks in which the grains are cemented together, the model is also practicable for in-cohesive granular materials. In fact, we can predict a modulus weakening effect similar to that reported in the existing literature (Espindola et al., 2012; Johnson and Jia, 2005) (data not shown) using this proposed model, simply by abandoning cohesion (i.e., $c = 0$).

The experiment conducted is analogous to field circumstances in which a seismic impact load affects the rock. Based on the parameters obtained, we can examine the dynamical weakening of the shallowly buried rock. Assume that the rock is under a hydrostatic state ($\sigma_r = \rho g h$ with $\rho = 2.3\, g/cm^3$, g = gravity acceleration and h = buried depth), hence the confining pressure is proportional to the depth. Although this condition is idealized due to the complex tectonic stress that may exist in the rock, it still can provide insights into the damage mechanism for such kind of rocks. The impact load is selected to be equivalent to 0.7 MPa releasing gas pressure (i.e., energy absorbed $E_a = 0.62$ J/cm^3), and the corresponding parameter μ is evaluated using the equation presented in Fig. 3(d). Figs. 4(c) and 4(d) show the influence of buried depth and impact number on dynamic modulus softening. When the velocity change exceeds 40% (corresponding to about a 60% modulus change), the rock will be damaged after the next impact load. Therefore, we define the critical state line as $\Delta M/M_0 = -0.6$, the cross-hatched region in Figs. 4(c) and 4(d), thus practically indicating a virtual state. If the material softening is related to weakening, the softening behavior shown in Figs. 4(c) and 4(d) can explain why the failure is not generated by the main shock of seismic waves, but rather by aftershocks (Huang et al., 2013). We take a rock located at a depth of 70 m as an example. After the rock is impacted three times, it remains at a critical state. If another shock (even a very small perturbation) occurs, the

stability will be lost and will induce the rock failure, and even sliding. The onset of land sliding triggered by consecutive impacts due to aftershocks or blasting, resulting in the rock weakening, can also be well interpreted. Influence of the number of impacts on dynamic weakening at different depths is presented in Fig. 4(d). The results show that a shallower buried rock is more inclined to damage after the impact by seismic waves.

In addition, a frequency spectrum analysis is used to characterize the impact loading nonlinear effect on the rock. A direct measurement of the specimen strain wave is difficult and may produce inaccurate results using the experimental facilities, thus we explore to study the spectra of the incident and transmitted waves using FFT analysis. Fig. 5(a) presents the typical waveforms of the incident and transmitted strain waves detected from the incident and transmission bars shown in Fig. 1(a) without specimens. It is clear that these two waveforms remain consistent and no waveform distortion is detected because of the extremely small nonlinear parameter of the bars. A neglected influence on the waveform distortion as observed in Fig. 5(d) is indicated. In addition, a trailing wave is found following the transmitted wave, a tensile wave induced by the interface reflection. Therefore, it is possible to explore the specimen nonlinear effect by examining the incident and transmitted waveforms due to impact, as shown in Figs. 5(c) and 5(d). The data are measured at the first impact under the conditions of 0.7 MPa releasing gas pressure and 2 MPa confining pressure. We band-pass filter the output signals at 3745 Hz, 2×3745 Hz, and 3×3745 Hz to analyze the frequency components of the incident and transmitted waves. In fact, the higher-order frequency components can also be found, but they are not initially evident because of the significantly small amplitudes. Obvious distortion is noticed by comparing the non-filtering transmitted wave with the incident wave due to the nonlinear

effect. To quantitatively account for harmonic waves, the frequency spectra for the incident and transmitted waves using FFT are presented in Fig. 5(b). The normalized magnitude of the second-order harmonic increases from 0.166 for the incident wave to 0.259 for the transmitted wave, and similar increases are also captured for the third- and fourth-order harmonic waves, which are induced by the energy transferred from low to high frequencies. Referring to the nonlinear wave model proposed by Brunet et al. (Brunet et al., 2008), the normalized magnitude of the second-order harmonic wave generated from the fundamental wave can be estimated as $\varepsilon_{2\omega}^{\text{nor.}} = \left(-\beta\omega\varepsilon_0 L\right)/\left(4C_0\right)$ with ε_0 as the strain wave amplitude (compressive strain is assumed as positive, $\varepsilon_0 = 10^{-2}$, for this experiment) and C_0 the linear wave velocity (measured as 2869 m/s). Here, we have neglected the attenuation induced by the internal dissipation for the sake of simplicity. Then, $\varepsilon_{2\omega}^{\text{nor.}}$ can be evaluated as 0.08 according to all known parameters, which is superposed on the original second-order harmonic wave with a normalized magnitude of 0.166, close to that of 0.259 for the transmitted wave. The same analysis can also be applied to higher-order harmonic waves.

With respect to a further insight on the non-filtering incident and transmitted waves, we found that the peak transmitted wave arrives at 104 μs, which is 8 μs prior to the arrival of the incident wave (i.e., 112 μs). The nonlinear wave velocity is known to be dependent on the strain wave amplitude ε_0, which is $C = C_0\left(1-\beta\varepsilon_0\right)$. For a travel distance of the specimen L, the time reduction can be evaluated as $\Delta t = L/C_0 - L/\left(C_0 - \beta\varepsilon_0 C_0\right) \approx 8.67\mu\text{s}$, which is very close to the observed result, i.e., 8 μs. The error might be induced by measurement accuracy because the sampling interval of our experimental facilities is 1 μs. We can further evaluate the travel distance for the formation of a shock wave as

$l_s = C_0/(\beta\omega\varepsilon_0) \approx 220\,\text{mm}$, which is larger than the wave traveling distance in the experiment. Hence, no shock wave is observed and no apparent wave distortion was observed in the previous experiment (Brunet et al., 2008) as the strain amplitude is in the order of 10^{-5}, inducing the wave velocity change by $(C - C_0)/C_0 = \beta\varepsilon_0 \approx -250\times10^{-5} = -0.25\%$, and thus it can be neglected.

Additional information can be extracted from the transmitted wave shown in Fig. 5(d), in which the appearance of a tensile wave is boxed with a dashed rectangle to indicate a significant plastic deformation after impact. This can be mistaken for a compression wave if solely inferred from the electrical signal recorded. Fig. 5(c) shows the wave duration is 266 μs, whereas the transmitted wave duration in Fig. 5(d) is 328 μs, which is 62 μs more. This extended time therefore corresponds to the tensile wave reflected from the interface of the specimen and transmission bar. Although only one example is selected here for nonlinear analysis, similar analyses for other cases (data not shown) can give the same results.

4 Conclusions

In summary, these analytical and experimental investigations show the nonlinear behavior of rocks subjected to high-amplitude impact loading. This can be described by the nonlinear dynamic model proposed by Johnson and Jia (2005), and the induced modulus softening can be accounted for by relating the energy absorbed to the modulus via a statistical model. The weakening process can be qualitatively captured only by introducing an energy-portion parameter μ into the present model, and it is further verified by comparing with the wave velocity measurement. Finally, we analyze the

nonlinear behavior using the frequency spectra of both incident and transmitted waves. It is concluded that the nonlinear theoretical predictions are consistent with the experimental observations, a convincing demonstration of the model proposed and developed in this work. Consequently, the weakening model proposed is capable of providing a deeper understanding of the failure evolution and mechanism of granular rocks and thus providing useful guidelines towards a better safety design and disaster prevention.

Acknowledgements:

The work described in this paper was supported by the National Natural Science Foundation of China (Grants No. 11602210 and 11702095), Jiangxi Science Fund for Distinguished Young Scholars (Grant No. 2018ACB21024), and the Matching Grant from the Hong Kong Polytechnic University (Project No. 4-BCDS).

References

Brown, E.T. (2012) Progress and challenges in some areas of deep mining. Mining Technology 121, 177-191. doi: 10.1179/1743286312Y.0000000012

Brunet, T., Jia, X., Johnson, P.A. (2008) Transitional nonlinear elastic behaviour in dense granular media. Geophysical Research Letters 35. doi:10.1029/2008GL035264

Chen, R., Li, K., Xia, K.W., Lin, Y.L., Yao, W., Lu, F.Y. (2016) Dynamic fracture properties of rocks subjected to static pre-load using notched semi-circular bend method. Rock Mech Rock Eng 49, 3865-3872. doi: 10.1007/s00603-016-0958-4

Chen, R., Yao, W., Lu, F., Xia, K. (2018) Evaluation of the Stress Equilibrium Condition in Axially Constrained Triaxial SHPB Tests. Exp Mech 58, 527-531. doi: 10.1007/s11340-017-0344-5

Dai, F., Xu, Y., Zhao, T., Xu, N.W., Liu, Y. (2016) Loading-rate-dependent progressive fracturing of cracked chevron-notched Brazilian disc specimens in split Hopkinson pressure bar tests. International Journal of Rock Mechanics and Mining Sciences 88, 49-60. doi: 10.1016/j.ijrmms.2016.07.003

Du, H.B., Dai, F., Xu, Y., Liu, Y., Xu, H.N. (2018) Numerical investigation on the dynamic strength and failure behavior of rocks under hydrostatic confinement in SHPB testing. International Journal of Rock Mechanics and Mining Sciences 108, 43-57. doi:10.1016/j.engfracmech.2017.09.001

Du, H.B., Dai, F., Xia, K.W., Xu, N.W., Xu, Y. (2017) Numerical investigation on the dynamic progressive fracture mechanism of cracked chevron notched semi-circular bend specimens in split Hopkinson pressure bar tests. Engineering Fracture Mechanics 184, 202-217. doi: doi.org/10.1016/j.ijrmms.2018.05.008

Espindola, D., Galaz, B., Melo, F. (2012) Ultrasound induces aging in granular materials. Physical Review Letters 109. doi: 10.1103/Physrevlett.109.158301

Frew, D.J., Akers, S.A., Chen, W., Mark, L.G. (2010) Development of a dynamic triaxial Kolsky bar. Measurement Science and Technology 21, 105704. doi: doi.org/10.1088/0957-0233/21/10/105704

Hokka, M., Black, J., Tkalich, D., Fourmeau, M., Kane, A., Hoang, N.H., Li, C.C., Chen, W.W., Kuokkala, V.T. (2016) Effects of strain rate and confining pressure on the compressive behavior of Kuru granite. International Journal of Impact Engineering

91, 183-193. doi: doi.org/10.1016/j.ijimpeng.2016.01.010

Huang, R., Zhao, J., Ju, N., Li, G., Lee, M.L., Li, Y. (2013) Analysis of an anti-dip landslide triggered by the 2008 Wenchuan earthquake in China. Natural Hazards 68:1021-1039. doi: 10.1007/s11069-013-0671-5

Huang, S., Mohanty, B., Xia, K. (2017) A multi-particle crushing apparatus for studying rock fragmentation due to repeated impacts. Rev Sci Instrum 88. doi: 10.1063/1.4993432

Jia, X. (2004) Codalike multiple scattering of elastic waves in dense granular media. Physical Review Letters 93. doi:10.1103/Physrevlett.93.154303

Johnson, P.A., Jia, X. (2005) Nonlinear dynamics, granular media and dynamic earthquake triggering. Nature 437: 871-874. doi: 10.1038/nature04015

Johnson, P.A., Savage, H., Knuth, M., Gomberg, J., Marone, C. (2008) Effects of acoustic waves on stick-slip in granular media and implications for earthquakes. Nature 451: 57-U55. doi: 10.1038/nature06440

Kaiser, P.K., Cai, M. (2012) Design of rock support system under rockburst condition. Journal of Rock Mechanics and Geotechnical Engineering 4:215-227. doi: doi.org/10.3724/SP.J.1235.2012.00215

Li, H., Xiang, X., Jianchun, L., Jian, Z., Bo, L., Yaqun, L. (2011) Rock damage control in bedrock blasting excavation for a nuclear power plant. International Journal of Rock Mechanics and Mining Sciences 48:210-218. doi: doi.org/10.1016/j.ijrmms.2010.11.016

Li, S.H., Zhu, W.C., Niu, L.L., Yu, M., Chen, C.F. (2018) Dynamic characteristics of green sandstone subjected to repetitive impact loading: Phenomena and mechanisms. Rock Mech Rock Eng 51:1921-1936. doi: 10.1007/s00603-018-1449-6

Li, X., Gong, F., Tao, M., Dong, L., Du, K., Ma, C., Zhou, Z., Yin, T. (2017) Failure mechanism and coupled static-dynamic loading theory in deep hard rock mining: A review. Journal of Rock Mechanics and Geotechnical Engineering 9:767-782. doi: doi.org/10.1016/j.jrmge.2017.04.004

Li, X., Zhou, Z., Lok, T.-S., Hong, L., Yin, T. (2008) Innovative testing technique of rock subjected to coupled static and dynamic loads. International Journal of Rock Mechanics and Mining Sciences 45:739-748. doi:

doi.org/10.1016/j.ijrmms.2007.08.013

Melosh, H.J. (1979) Acoustic fluidization: A new geologic process? Journal of Geophysical Research Solid Earth 84:7513-7520. doi: doi.org/10.1029/JB084iB13p07513

Melosh, H.J. (1996) Dynamical weakening of faults by acoustic fluidization. Nature 379: 601-606. doi:10.1038/379601a0

Potyondy, D.O., Cundall, P.A. (2004) A bonded-particle model for rock. International Journal of Rock Mechanics and Mining Sciences 41:1329-1364. doi: doi.org/10.1016/j.ijrmms.2004.09.011

Weng, L., Li, X., Taheri, A., Wu, Q., Xie, X. (2018) Fracture evolution around a cavity in brittle rock under uniaxial compression and coupled static-dynamic loads. Rock Mechanics & Rock Engineering 51:1-15. doi: 10.1007/s00603-017-1343-7

Wu, B.B., Kanopoulos, P., Luo, X.D., Xia, K.W. (2014) An experimental method to quantify the impact fatigue behavior of rocks. Measurement Science and Technology 25. doi: 10.1088/0957-0233/25/7/075002

Wu, B.B., Yao, W., Xia, K.W. (2016) An experimental study of dynamic tensile failure of rocks subjected to hydrostatic confinement. Rock Mech Rock Eng 49:3855-3864. doi: 10.1007/s00603-016-0946-8

Xia, K., Yao, W. (2015) Dynamic rock tests using split Hopkinson (Kolsky) bar system – A review. Journal of Rock Mechanics and Geotechnical Engineering 7:27-59. doi: doi.org/10.1016/j.jrmge.2014.07.008

Xia, K.W., Huang, S., Marone, C. (2013) Laboratory observation of acoustic fluidization in granular fault gouge and implications for dynamic weakening of earthquake faults. Geochem Geophy Geosy 14:1012-1022. doi: 10.1002/ggge.20076

Xu, Y., Dai, F. (2018) Dynamic response and failure mechanism of brittle rocks under combined compression-shear loading experiments. Rock Mech Rock Eng 51:747-764. doi: 10.1007/s00603-017-1364-2

Xu, Y., Dai, F., Xu, N.W., Zhao, T. (2016) Numerical investigation of dynamic rock fracture toughness determination using a semi-circular bend specimen in Split Hopkinson pressure bar testing. Rock Mech Rock Eng 49:731-745. doi: 10.1007/s00603-015-0787-x

Zhou, Y.X., Xia, K., Li, X.B., Li, H.B., Ma, G.W., Zhao, J., Zhou, Z.L., Dai, F. (2012)

Suggested methods for determining the dynamic strength parameters and mode-I fracture toughness of rock materials. International Journal of Rock Mechanics and Mining Sciences 49:105-112. doi: 10.1016/j.ijrmms.2011.10.004

Zhu, W.C., Bai, Y., Li, X.B., Niu, L.L. (2012) Numerical simulation on rock failure under combined static and dynamic loading during SHPB tests. International Journal of Impact Engineering 49:142-157. doi: doi.org/10.1016/j.ijimpeng.2012.04.002

Caption of Figures

Fig. 1 (a) Experimental setup; (b) A typical specimen; and (c) Typical incident, reflected and transmitted waveforms.

Fig. 2 (a) to (c): Dynamic stress-strain curves for a releasing gas pressure of 0.7 MPa. (d) to (f): Dynamic stress-strain curves for a releasing gas pressure of 0.9 MPa. (N is the number of impact).

Fig. 3 Energy absorbed for a releasing gas pressure of (a) 0.7 MPa and (b) 0.9 MPa. The inset figure in (b) shows that the average energy absorbed under various confining pressure. (c) Variation of the nonlinear parameters β and δ versus the impact number. (d) Variation of the fitted parameter μ versus the confining pressure.

Fig. 4 Effect of the impact number on the normalized velocity change for a releasing gas pressure of (a) 0.7 MPa and (b) 0.9 MPa. Variation of the normalized dynamic modulus with (c) the buried depth under various impact numbers; and (d) the impact number under different buried depths of the field rock.

Fig. 5 (a) Incident and transmitted strain waves without specimens at a releasing gas pressure of 0.7 MPa for reference. (b) A frequency spectrum of both incident and transmitted waves. Frequency components at the first-, second- and third-order of the incident wave (c) and transmitted wave (d).

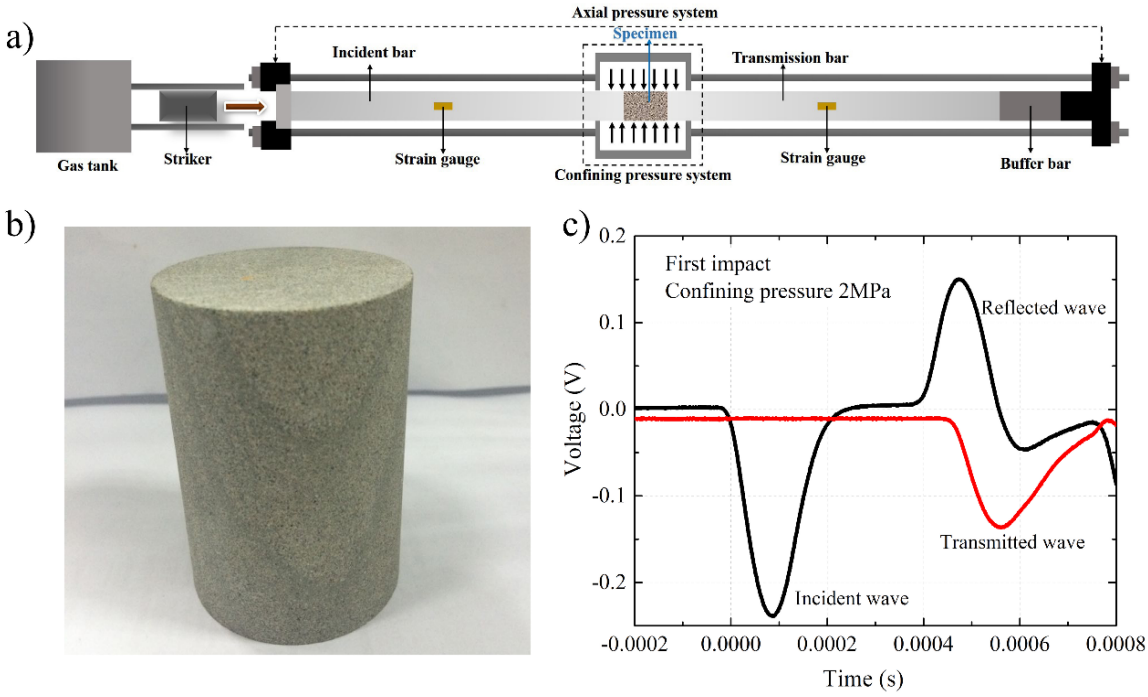

Fig. 1 (a) Experimental setup; (b) A typical specimen; and (c) Typical incident, reflected and transmitted waveforms.

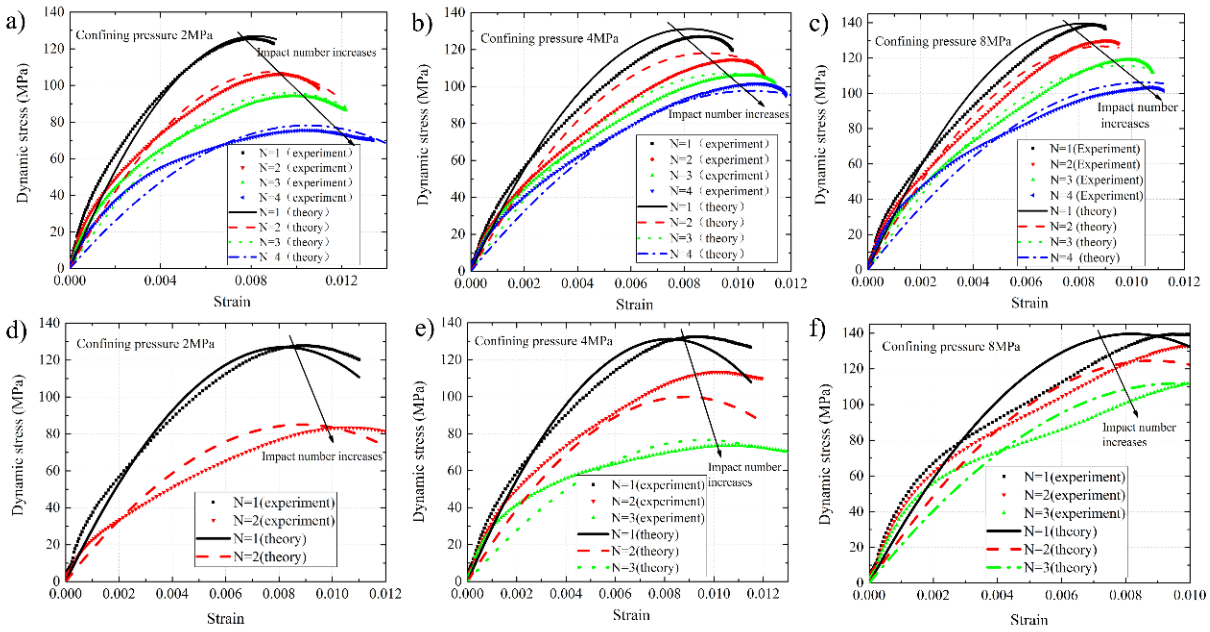

Fig. 2 (a) to (c): Dynamic stress-strain curves for a releasing gas pressure of 0.7 MPa. (d) to (f): Dynamic stress-strain curves for a releasing gas pressure of 0.9 MPa. (*N* is the number of impact).

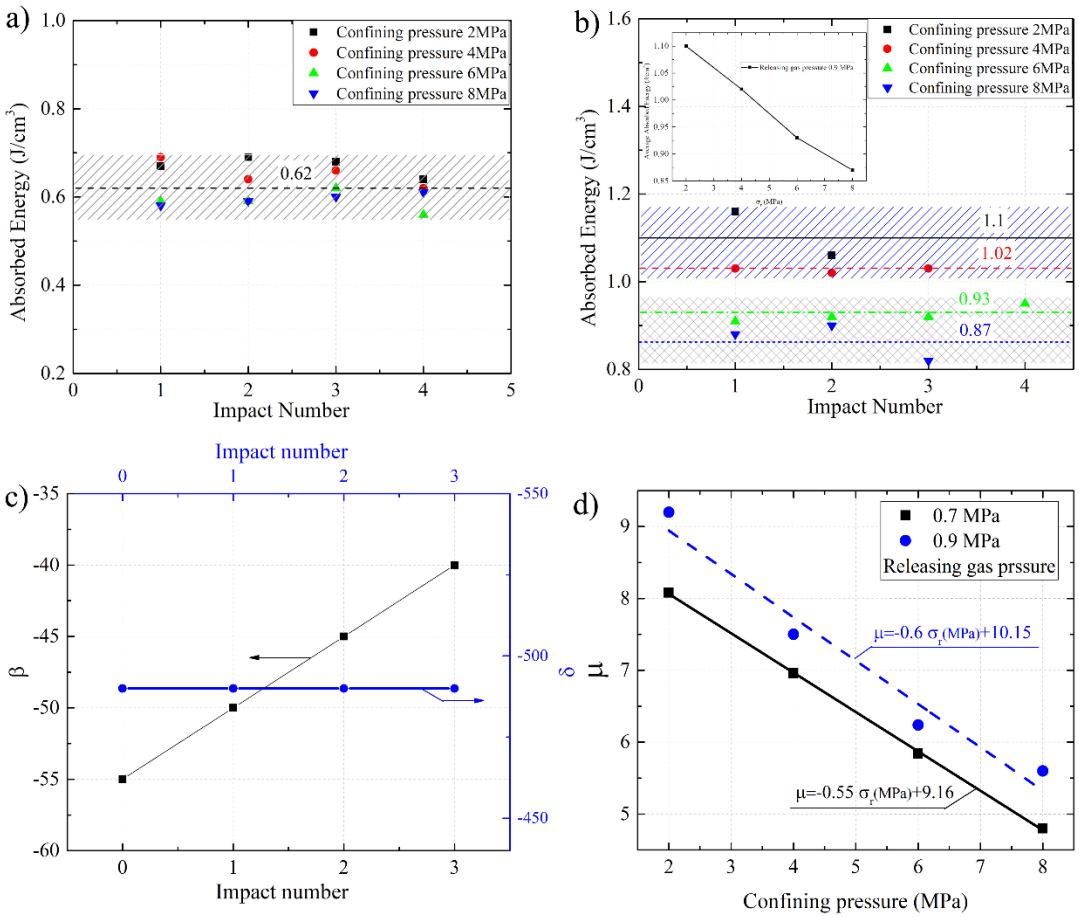

Fig. 3 Energy absorbed for a releasing gas pressure of (a) 0.7 MPa and (b) 0.9 MPa. The inset figure in (b) shows that the average energy absorbed under various confining pressure. (c) Variation of the nonlinear parameters β and δ versus the impact number. (d) Variation of the fitted parameter μ versus the confining pressure.

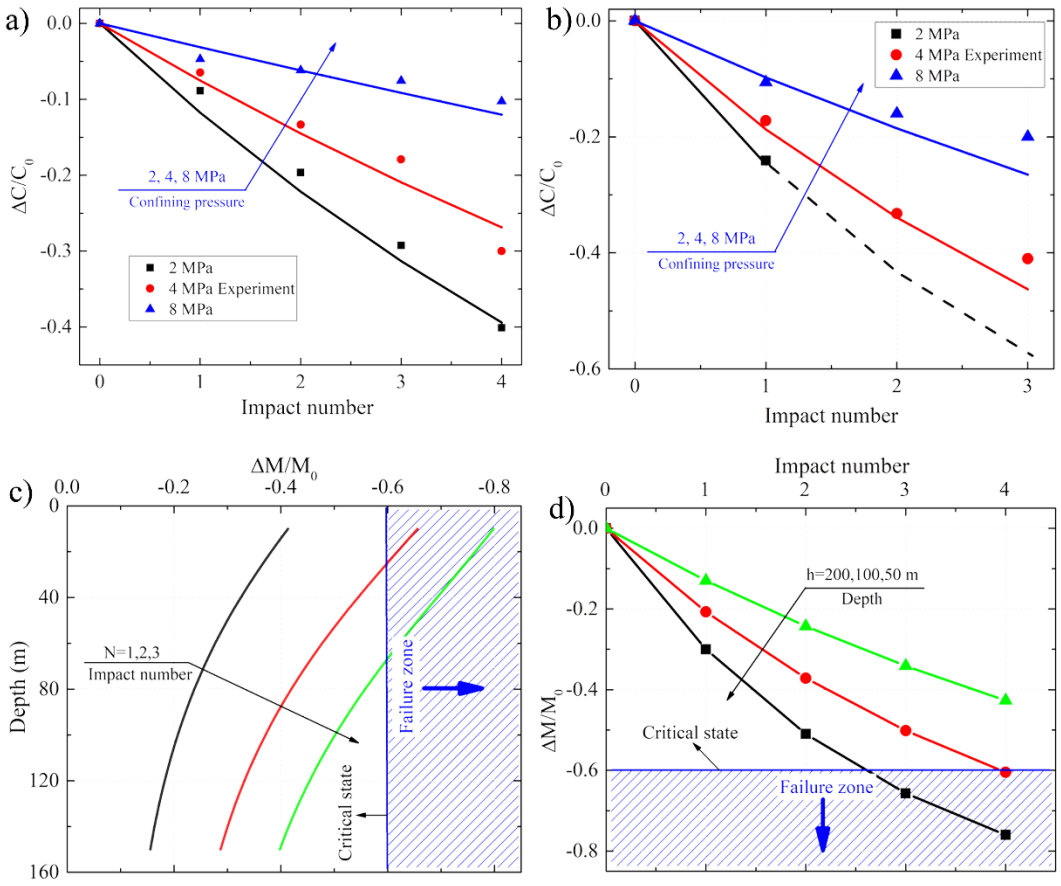

Fig. 4 Effect of the impact number on the normalized velocity change for a releasing gas pressure of (a) 0.7 MPa and (b) 0.9 MPa. Variation of the normalized dynamic modulus with (c) the buried depth under various impact numbers; and (d) the impact number under different buried depths of the field rock.

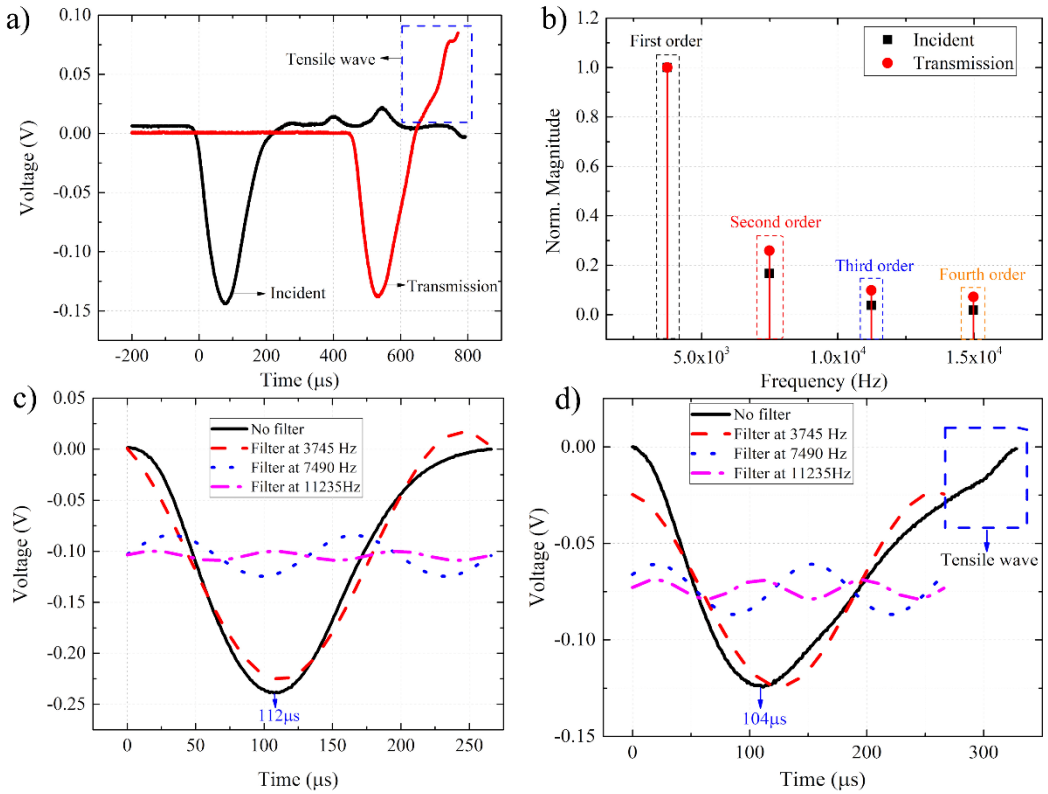

Fig. 5 (a) Incident and transmitted strain waves without specimens at a releasing gas pressure of 0.7 MPa for reference. (b) A frequency spectrum of both incident and transmitted waves. Frequency components at the first-, second- and third-order of the incident wave (c) and transmitted wave (d).